Investigation of metal interactions with YrpE protein of *Bacillus subtilis* by a polyhistidine peptide model

Denise Bellotti [a],[b],[*], Silvia Leveraro [a], Aleksandra Hecel [b], Maurizio Remelli [a]

[a] *Department of Chemical, Pharmaceutical and Agricultural Sciences, University of Ferrara, 44121, Ferrara, Italy*
[b] *Faculty of Chemistry, University of Wrocław, 50-383, Wrocław, Poland*

ARTICLE INFO

ABSTRACT

The use of model peptides that can simulate the behaviour of a protein domain is a very successful analytical method to study the metal coordination sites in biological systems. Here we study zinc and copper binding ability of the sequence HTHEHSHDHSHAH, which serves as model for the metal interactions with YrpE, a putative metal-binding protein of the ZinT family identified in *Bacillus subtilis*. Compared to other ZinT proteins secreted by Gram-negative bacteria, the metal-coordination properties of YrpE N-terminal histidine-rich domain have not been yet characterized. Different independent analytical methods, aimed at providing information on the stability and structure of the formed species, have been employed, including potentiometric titrations, electrospray ionization mass spectrometry, UV–Vis spectrophotometry, circular dichroism and electron paramagnetic resonance spectroscopy. The obtained speciation models and equilibrium constants allowed to compare the metal-binding ability of the investigated polyhistidine sequence with that of other well-known histidine-rich peptides. Our thermodynamic results revealed that the YrpE domain HTHEHSHDHSHAH forms more stable metal complexes than other His-rich domains of similar ZinT proteins. Moreover, the studied peptide, containing the alternated $(-XH-)_n$ motif, proved to be even more effective than the His6-tag (widely used in immobilized metal ion affinity chromatography) in binding zinc ions.

1. Introduction

Studying protein systems can be a very difficult task, especially if the dynamic and environmentally dependent nature of the metal-protein interaction is considered. A complete comprehension of the system requires a high number of analyses performed under different experimental conditions and eventually implies the description of the species distribution, the ligand coordination modes, complex stoichiometry and geometry. In the last decades a very successful analytical procedure suitable to study metal interaction in biological systems has been developed [1–3]. This method is aimed at simplifying the experimental investigation using model peptides which mimic the metal coordination sites in native protein. The choice of the model peptide is a crucial step, and it is guided by two main requirements: (i) the behaviour of the metal binding domain should be only negligibly affected by the rest of the protein; (ii) the model peptide sequence is unstructured both within the protein in its biological environment and as "free" ligand under the investigated experimental conditions. The valuable feature of the analytical method based on model peptides concerns not only the

simplification of the metal-protein interaction investigation, but also the chance to deepen the knowledge on the properties of different peptides and their metal complexes. Such information can be employed in many other applications, *e.g.* design of antimicrobial agents, metal decontamination, immobilized metal ion affinity chromatography. In this work we use a model peptide to better understand the cellular metal acquisition process of *Bacillus subtilis*, a Gram-positive bacterium isolated from various soil and marine environments, also found in the gastrointestinal tract of humans [4,5]. Due to its ease of genetic manipulation and widespread use in many areas, including industry, it is one of the most well-studied bacteria, often used as model organism. The fortune of *B. subtilis* arises from its extraordinary versatility, that makes it useful for various applications from enzyme production and food fermentation to environmental decontamination and aquaculture [6–9].

B. subtilis is routinely used in wastewater treatment [10,11] and in bioremediation processes [12,13], thanks to its ability to remove organic wastes, heavy metals and other contaminants [14,15]. The interaction with metal ions is a key aspect of *B. subtilis* technological and medical applications [16]. It proved to be effective in heavy metal

remediation, providing an environmentally friendly approach to enhance the uptake of cadmium, lead, copper, zinc, nickel, arsenic and mercury [16]. Several studies also show that *B. subtilis* biofilm formation is strictly affected by the presence of metal ions which can be absorbed by the biofilm matrix and change its properties [17,18]. However, *B. subtilis*, as any other organism, requires a tight regulation of metal ion homeostasis. Metalloregulatory proteins of different families (*e.g.* Fur, DtxR, MerR, and ArsR/SmtB) are therefore in charge of sensing cytosolic metal levels and direct metal ion uptake, storage and efflux [19]. Given the importance of metal interaction with *B. subtilis* cells, the mechanisms of metal homeostasis require an extensive study [15,19].

The genome analysis of *B. subtilis* has revealed the presence of a candidate component of the ATP binding cassette (ABC) transporter, here called YrpE. It supposedly functions as a zincophore, *i.e.* a specialised zinc chelator able to catch the metal from the colonized environment and transfer it to an appropriate target protein (most often a transmembrane transporter) [20,21]. In many bacteria, the extracellular component of zinc specific ABC transporters can cooperate with an additional protein to increase the efficiency of zinc recruitment: it is the case of the periplasmic proteins ZinT [22] and AztD [23] or of the pneumococcal histidine triad protein PhtD [24]. The mechanisms by which the paired proteins interact are still uncertain, depending on the involved systems and on the considered microorganism [25].

The predicted zinc-binding protein YrpE of *B. subtilis* shows high similarities with the ZinT protein of *Escherichia coli* and *Salmonella enterica* (45% of sequence identity, Scheme S1). These proteins belong to the same ZinT protein family and contain regions abundant with histidine and aspartic and glutamic acid residues in their N-terminal domain [26]. Histidine amino acid is particularly known for its propensity to bind metals like Zn^{2+} and Cu^{2+} [3,27,28]. Noteworthy, the comparison of YrpE (*B. subtilis*) and ZinT (*E. coli, S. enterica*) shows a main difference in the N-terminal domain, where the His-rich loop characteristic of ZinT protein family is located. In the case of YrpE protein from *B. subtilis* the His-rich loop corresponds to the 13-mer fragment between residues 57 and 69 (Scheme S1).

According to the predicted three-dimensional structure provided by AlphaFold software v2.0 [29] and UniProt Database (UniProt identifier: O05410) [30], the identified fragment does not present any specific structural conformation, and it can be therefore converted in a perfect model peptide to study the metal interaction with this protein domain. Analogously, the thermodynamic characterization of metal complexes with model peptides corresponding to the flexible His-rich loop of ZinT proteins from *E. coli* and *S. enterica* (residues 24–29, -HXHHXH-) suggested its role in zinc sequestration from the surrounding environment [31]. A similar study for ZinT-like protein in Gram-positive bacteria is missing, prompting us to investigate the putative zinc-binding protein YrpE from the model organism *B. subtilis*. Comparing the flexible His-rich loop of YrpE from *B. subtilis* (a Gram-positive bacterium) and that of the ZinT proteins from *E. coli* and *S. enterica* (two Gram-negative bacteria), we would like to highlight the possible differences in the metal binding ability. Indeed, in the case of YrpE, the sequence is longer and characterized by a zinc-binding motif with seven alternated histidine residues (-HTHEHSHDHSHAH-). Hence, the question is: how the number and position of the histidine residues affect the zinc binding efficacy of this N-terminal loop in YrpE/ZinT proteins?

To answer the question, the acid-base properties of the peptide Ac-HTHEHSHDHSHAH-NH₂, corresponding to the sequence 57–69 of the YrpE protein, have been characterized by potentiometry at a given temperature and ionic strength. The ability to form zinc(II) and copper (II) complexes has also been deeply investigated by means of different techniques, including potentiometric titrations in the pH range 2–11, UV–Vis absorption spectrophotometry, mass spectrometry (MS), circular dichroism (CD) and electron paramagnetic resonance (EPR). Zinc has been selected because it is the primary substrate for the chosen protein. Nevertheless, many examples in literature show that copper ion can efficiently compete for the same zinc binding sites, and both these

metals are essential micronutrients for *B. subtilis* and can be absorbed from the extracellular environment [13,19,32].

Another crucial point concerns the importance of polyhistidine peptides in many applications. Almost 80% of histidine-rich proteins have been found in bacteria, and around 33% of their totality contains polyhistidyl motifs. Polyhistidyl sequences have been reported to form relatively strong interactions with transition metal ions (Ni^{2+}, Cu^{2+}, Zn^{2+} and Co^{2+}) mostly thanks to the imidazole ring of the histidine side-chain [33]. His-rich peptides also proved to be involved in antimicrobial activities, examples include histatins [34], calcitermin [35], piscidins [36], shepherin [37] and clavanins [38], where histidine residues are present in number from 3 to 8 and occupy different positions. In recent years, histidine-rich antimicrobial peptides have been suggested to participate in the mechanism known as nutritional immunity, *i.e.* the process by which an organism withdraws essential metal ions in order to limit their bioavailability and reduce the pathogenicity during infections [39,40]. The position of histidine residues may therefore affect the efficacy of the metal coordination. Interestingly, the peptide investigated in this work (Ac-HTHEHSHDHSHAH-NH₂) is formed by 7 alternated histidines separated by only one amino acid. Comparing its Zn^{2+} and Cu^{2+} binding affinity with that of other His-rich peptides can therefore highlight its potential as metal chelator. Nevertheless, such information is also useful for other purposes, for example immobilized metal ion affinity chromatography (IMAC) [41,42], where the basic tool for purification of the recombinant proteins are hexa-histidine affinity tags (-HHHHHH-), alternated histidine-glutamine and histidine-asparagine tags [43], or other natural derived polyhistidine tags [44]. Due to their special metal binding properties, poly-His peptides can therefore be exploited for various applications aimed at sensing and trapping metals.

2. Results

2.1. Ligand protonation

The acid-base properties of peptide Ac-HTHEHSHDHSHAH-NH₂ have been studied by potentiometric titrations. The ligand contains two acidic residues, Asp and Glu, which can release a proton from their carboxylic side chain. In addition to these acidic residues, the peptide contains seven alternated histidine residues, which participate in acid-base equilibria through the imidazole ring of their side chains. The obtained protonation constants are reported in Table 1. The release of acidic protons from Asp and Glu residues occurs with a dissociation constant of 3.02 and 3.98, respectively. According to literature [45] we assigned the lower value to the aspartic acid, which is generally more acidic than the glutamic acid.

The subsequent deprotonation steps are due to the seven His residues. The log$K$ values of the side imidazole groups of histidines spans in the range 5.48–7.54, in agreement with literature [45]. The available data do not allow to exactly attribute a protonation value to every single His residue in terms of *micro*-constants. However, the acidity of protonated histidines decreases (and the step protonation constant grows) as the charge of the peptide decreases (due to the progressive loss of protons in a more and more basic environment) until becoming negative.

2.2. Formation of metal complexes in solution

The alternated histidyl-tag is of particular importance for metal coordination and is supposed to bind divalent metal ions like Cu^{2+} and Zn^{2+} with high efficacy. Nevertheless, a thorough investigation of the thermodynamic and spectroscopic properties of metal/ligand (M/L) complex formation is crucial to understand the role of this protein fragment and to compare it with other metal chelating sequences diffused in natural proteins and peptides.

As reported in the Experimental section, the thermodynamic

Table 1

Equilibrium constants and proposed coordination modes for Cu^{2+} and Zn^{2+} complexes with ligand Ac-HTHEHSHDHSHAH-NH$_2$, $T = 298$ K, $I = 0.1$ M (NaClO$_4$) and M:L molar ratio = 0.9:1. Values in parentheses are standard deviations on the last significant figure.

Species	logβ	pK_a	Metal coordination
Ligand protonation			
H_9L^{7+}	51.94(6)	3.02	
H_8L^{6+}	48.92(4)	3.98	
H_7L^{5+}	44.94(4)	5.48	
H_6L^{4+}	39.47(2)	5.65	
H_5L^{3+}	33.81(3)	6.25	
H_4L^{2+}	27.56(2)	6.26	
H_3L^+	21.30(3)	6.77	
H_2L	14.53(1)	6.99	
HL^-	7.54(2)	7.54	
Cu^{2+} complexes			
$[CuH_5L]^{5+}$	40.04(3)	4.45	2N$_{Im}$
$[CuH_4L]^{4+}$	35.59(3)	4.92	3N$_{Im}$
$[CuH_3L]^{3+}$	30.67(3)	5.91	4N$_{Im}$
$[CuH_2L]^{2+}$	24.76(4)	6.23	4N$_{Im}$, N$_{Im(ax)}$
$[CuHL]^+$	18.53(3)	7.68	4N$_{Im}$, N$_{Im(ax)}$
$[CuL]$	10.85(5)	8.42	4N$_{Im}$, N$_{Im(ax)}$
$[CuH_{-1}L]^{1-}$	2.43(6)	8.46	3N$_{Im}$, N$^-$, N$_{Im(ax)}$
$[CuH_{-2}L]^{2-}$	−6.03(4)	9.47	2N$_{Im}$, 2N$^-$, N$_{Im(ax)}$
$[CuH_{-3}L]^{3-}$	−15.50(4)		N$_{Im}$, 3N$^-$, N$_{Im(ax)}$
Zn^{2+} complexes			
$[ZnH_3L]^{3+}$	27.06(6)	5.47	4N$_{Im}$
$[ZnH_2L]^{2+}$	21.59(4)	6.20	4-5N$_{Im}$
$[ZnHL]^+$	15.40(6)	7.25	4N$_{Im}$
$[ZnL]$	8.15(7)		4N$_{Im}$

Fig. 2. Species distribution diagram of Zn^{2+}/Ac-HTHEHSHDHSHAH-NH$_2$; metal:ligand ratio 0.9:1; $C_L = 1 \cdot 10^{-3}$ M.

investigation of complex-formation equilibria has been performed by means of potentiometric titrations on solutions where the metal:ligand stoichiometric ratio was M:L = 0.9:1. The speciation models for the M/L systems are reported in Table 1, and the corresponding species distribution diagrams are depicted in Figs. 1 and 2. In the case of Cu^{2+} complexes, for which spectroscopic investigations were informative, UV–Vis and CD data are summarised in Fig. 3 and EPR data are reported in Table S1 and Fig. S1.

For both copper and zinc complexes, the high-resolution mass spectra (Figs. S2 and S3) reveal the formation of only mononuclear species under the employed experimental conditions. The most intense detected signals correspond to metal complexes at different protonation states and/or their sodium and potassium adducts, as shown in Figs. S2 and S3. No poly-nuclear complexes or bis-complexes are identified. The obtained MS profiles for the M/L systems are in accordance with the
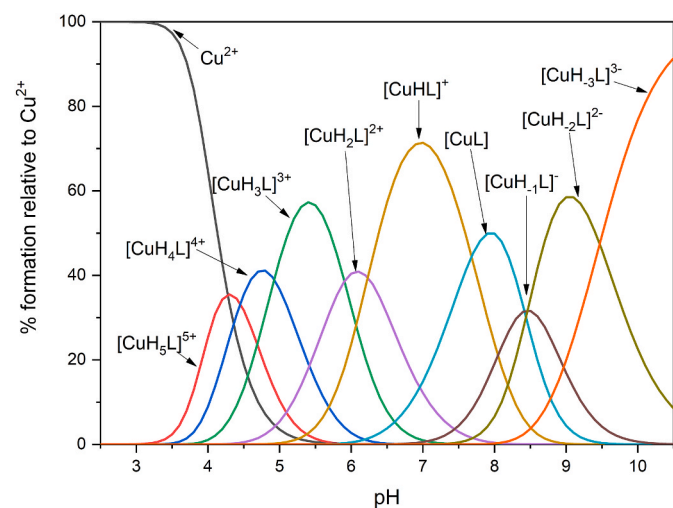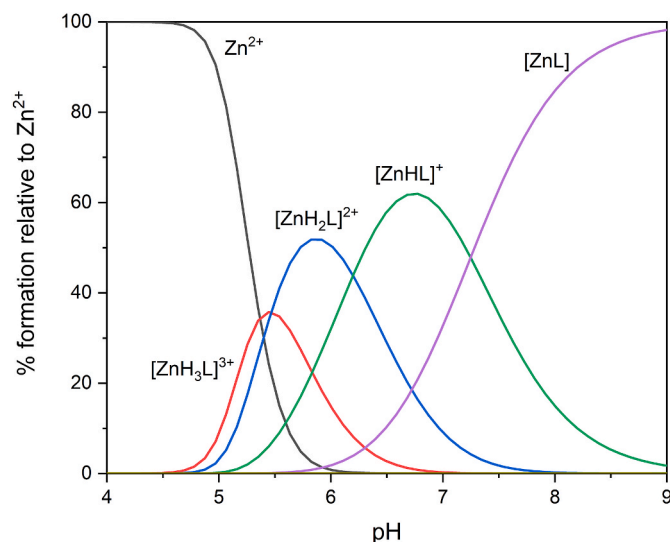
speciation models reported in Table 1, which also outline the prevalence in solution of 1:1 metal complexes.

Copper ion interacts with Ac-HTHEHSHDHSHAH-NH$_2$ ligand from pH 3, forming nine different species in solution in the explored pH range (Fig. 1). The first complex, $[CuH_5L]^{5+}$, is likely characterized by a (2N$_{Im}$) coordination, where two histidine residues are bound to the metal center through their imidazole side chains. Although it is reasonable to consider the participation of the carboxylic groups of Asp and/or Glu residues in the coordination, such hypothesis is not supported by the wavelength of maximum absorption recorded at pH 4.3, where $[CuH_5L]^{5+}$ reaches its maximum of formation in solution: the experimental λ_{max} value (681 nm) suggests a (2N$_{Im}$) binding mode (expected λ_{max}: 685 nm [46]). The remaining coordination positions of the octahedron are occupied by water molecules. When pH is increased, the species $[CuH_4L]^{4+}$ is formed. It is characterized by a pK_a value of 4.45. This value can describe the proton release from a histidine residue which substitutes a water molecule in the metal coordination sphere. Analogously, the next deprotonation step (pK_a = 4.92) suggests the coordination of a fourth histidine to obtain the (4N$_{Im}$) complex $[CuH_3L]^{3+}$, which reaches its maximum of formation around pH 5.5. The release of a further proton (pK_a = 5.91) to form $[CuH_2L]^{2+}$ is again ascribed to the metal interaction with a histidine residue, which enters the coordination sphere and likely occupies an axial position. This hypothesis is supported by the obtained UV–Vis absorption data. In fact, the obtained wavelength of maximum absorption in the pH range 6–8 is slightly higher than that expected for a 4N$_{Im}$ complex (experimental λ_{max} = 585 nm, expected λ_{max} = 575 nm) and may be due to the presence of axial donor groups. Axial interactions usually induce a shift towards longer wavelengths [46]. Moreover, given the unchanged spectroscopic properties in the pH range 6–8 where $[CuH_2L]^{2+}$, $[CuHL]^+$ and $[CuL]$ species are formed in solution, it is reasonable to suggest the same coordination mode for these three complexes. As a consequence, the corresponding deprotonation constants should refer to two histidine residues which do not participate in the complexation. This is also supported by EPR results, since no changes in the A∥ and g∥ values have been detected in the same pH range (Table S1). Moving to alkaline conditions, instead, UV–Vis, CD and EPR spectra undergo significant changes (Fig. 3 and S1). In fact, we can observe a decrease of the wavelength of maximum absorption in UV–Vis spectra from 585 nm to 532 nm (Fig. 3a), and an increase of the CD signals (Fig. 3b), particularly in the Vis range (400–800 nm). Such behaviour is well known for copper chelating peptides, and it is indicative of the coordination of the amide
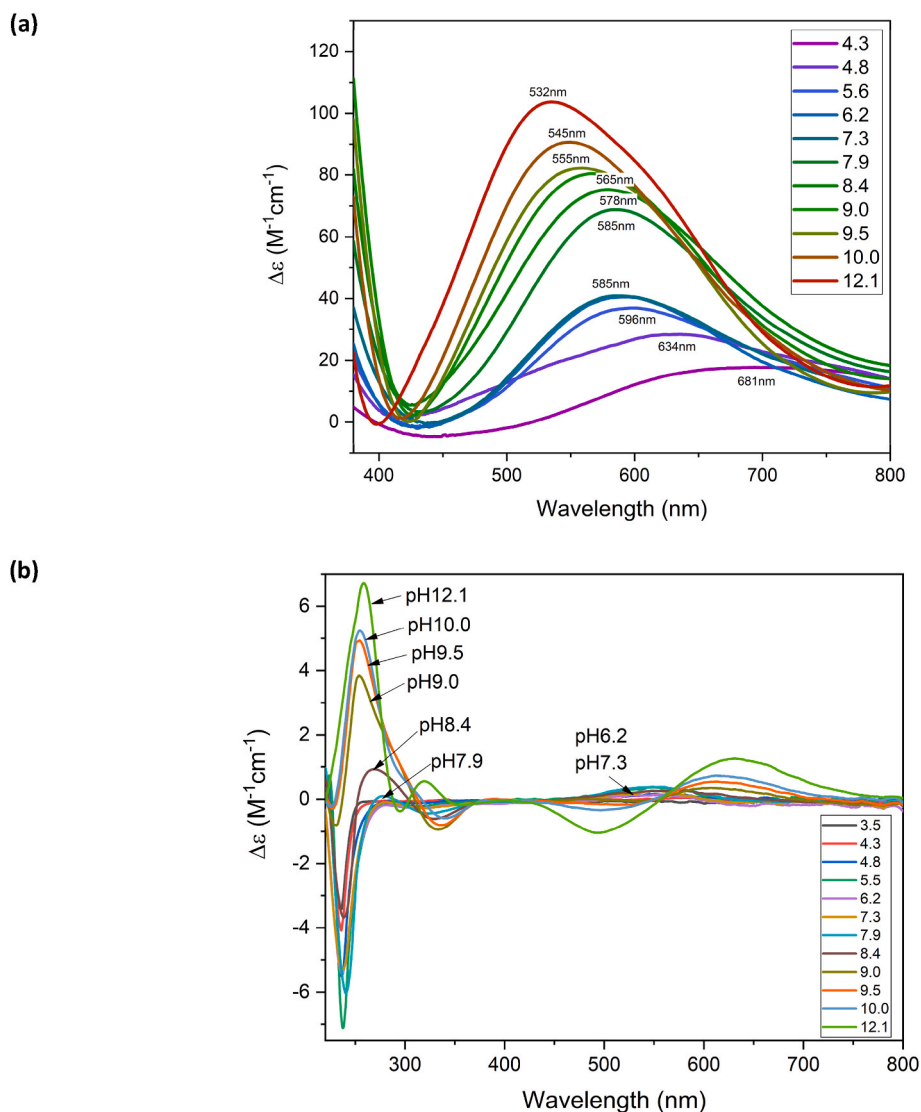

Fig. 1. Species distribution diagram of Cu^{2+}/Ac-HTHEHSHDHSHAH-NH$_2$; metal:ligand ratio 0.9:1; $C_L = 1 \cdot 10^{-3}$ M.

(a)

(b)

Fig. 3. (a) Vis absorption spectra, (b) CD spectra of Cu^{2+}/Ac-HTHEHSHDHSHAH-NH_2 system.

nitrogens of the peptide backbone [3,47,48]. The N-amides can substitute the imidazole donor groups in the equatorial plane of the complex, increasing its square planar character. It is the case of the species $[CuH_{-1}L]^{-1}$, $[CuH_{-2}L]^{-2}$ and $[CuH_{-3}L]^{-3}$, which are characterized by pK_a values of 8.42, 8.46 and 9.47, respectively (Table 1). For these complexes we can therefore suggest, in the order, a ($3N_{Im}$, N^-), ($2N_{Im}$, $2N^-$) and (N_{Im}, $3N^-$) binding mode. An axial interaction with the side chain of

histidines is also conceivable (Fig. 4), as indicated by a slight red-shift ($\approx$15 nm) of the experimental λ_{max} with respect to the expected ones, where only equatorial donor groups are considered.

The formation of zinc complexes with Ac-HTHEHSHDHSHAH-NH_2 ligand begins at pH 4.5. Four zinc complexes with different protonation states are formed in solution up to pH 9 (Fig. 2), condition where precipitation was observed in solution. The first identified species at the
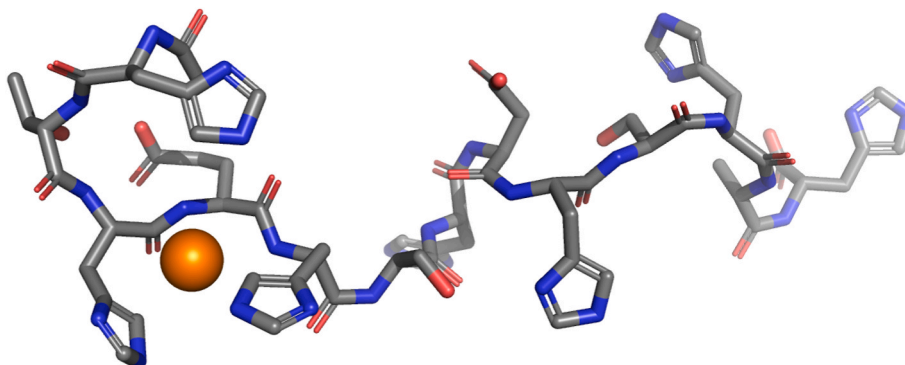

Fig. 4. Schematic model of the ($2N_{Im}$, $2N^-$, axial N_{Im}) binding mode for Cu^{2+} ion.

most acidic pH values is $[ZnH_3L]^{3+}$. According to its stoichiometry, the ligand has already lost six protons, most likely released by the two acidic residues, Asp and Glu, and four histidines. All these residues represent possible donor groups for the Zn^{2+} ion and can participate in the complex-formation process (Fig. 5). Increasing the pH value, the formation of three further complexes occurs: $[ZnH_2L]^{2+}$, $[ZnHL]^+$ and $[ZnL]$. The corresponding thermodynamic constants support the release of the acidic proton from the protonated imidazole side chain of the remaining three histidine residues. Given the high number of potential donor groups and the conformational flexibility of Zn^{2+} ion, we cannot exclude the formation of a mixture of complexes with different geometries. The bound histidines can mutually exchange with another imidazole group, forming tetra- or penta-coordinated systems with distorted tetrahedral or pyramidal arrangements, respectively [49,50].

Lastly, the three-dimensional structure adopted by the peptide in solution has been studied by means of circular dichroism in the range 180–260 nm (Fig. S4). The conformation remains unchanged after the formation of metal complexes, and it is prevalently random coil in aqueous solution.

3. Discussion

3.1. The N-terminal His-rich domain of YrpE binds zinc and copper with higher affinity than the corresponding sequences in ZinT protein

The investigated Ac-HTHEHSHDHSHAH-NH$_2$ ligand corresponds to the flexible His-rich loop, highly conserved in ZinT-like proteins. This domain is supposed to strongly interact with metal ions, acting as primary metal scavenger. Such behaviour has been proved for ZinT protein secreted by *E. coli* (*Ec*ZinT) and *S. enterica* (*Se*ZinT), where the unstructured N-terminal metal binding-site corresponds to the sequence 24–29, -HGHHXH- (X = Ser in *Ec*ZinT and X = Ala in *Se*ZinT) [31]. YrpE is classified as a protein of ZinT family; however, a remarkable difference from *Ec*ZinT and *Se*ZinT concerns this His-rich domain. It is longer and contains a higher number of histidine residues arranged in an alternated motif. We therefore decided to compare the flexible loop of YrpE and ZinT proteins to better understand its role on the basis of the Gram-negative and Gram-positive classification of bacteria. The competition diagram in Fig. 6 shows that HTHEHSHDHSHAH sequence is more effective than HGHHXH in binding Zn^{2+} and Cu^{2+} until pH 8. This means that in a common biological environment (physiological and/or acidic pH), YrpE displays a better ability to catch metal ions. This behaviour is explained by the higher number of histidines in Ac-HTHEHSHDHSHAH-NH$_2$, which allows a higher number of conformations with different sets of bound imidazoles. We can suggest that the remarkable difference in metal-binding affinity between YrpE and ZinT, highlighted by our thermodynamic investigations (Fig. 6), arises from the different niches where these proteins operate. In the first case, being *B. subtilis* a Gram-positive bacterium, YrpE is likely located on the cell surface and is exposed to the extracellular environment [26]. Its flexible

Fig. 5. Schematic model of the (4N$_{Im}$) binding mode for Zn^{2+} ion.

loop in charge of metal recruitment must therefore compete with several metal chelators participating in the host nutritional immunity. ZinT is instead located in the periplasm of Gram-negative bacteria and interacts with metal ions already internalized through the outer membrane. The severe competitiveness to which YrpE is subjected may be responsible for the higher metal-binding affinity of its N-terminal His-rich loop.

The alternated (HX)$_n$ histidyl tag of Ac-HTHEHSHDHSHAH-NH$_2$ is a very effective binding motif for zinc ion.

Polyhistidine peptides are extremely important in many applications which involve the coordination of metal ions, being also quite diffused in nature and as antimicrobial agents. However, differences in the position and number of histidines may strongly influence the metal-binding ability of the peptide. We therefore tried to compare the zinc- and copper-binding affinity of two different alternated histidyl motifs. The -(XH)$_7$- polyhistidine sequence of Ac-HTHEHSHDHSHAH-NH$_2$, where each histidine is separated by one residue, has been compared to the polyhistidine sequence of the Prion protein of zebrafish, Ac-PVHTGHMGHIGHTGHTGHTGSSGHG-NH$_2$ (zp-PrP63-87), which also contains seven histidines but with a different alternated motif -(XXH)$_6$-XXXXXH- [51,52] (Fig. 7). No significative differences are observed for the formation of Cu^{2+} complexes, since both the peptides coordinate the metal with comparable efficacy until pH 9. The same is not verified for Zn^{2+}, where the -(HX)$_7$- motif promotes the formation of stable complexes. This result suggests that peptides where multiple histidines are separated by only one amino acid are better zinc chelators than those with two residues between each histidine, even though the coordination modes are the same.

To further verify this assumption, we compared Ac-HTHEHSHDHSHAH-NH$_2$ with the well-known hexa histidine-tag -HHHHHH-, which is used in immobilized metal ion affinity chromatography thanks to its capacity to form stable complexes with many metal cations, including Zn^{2+} and Cu^{2+} [28,33]. The competition diagrams depicted in Fig. 8 compare the capacity of Ac-HTHEHSHDHSHAH-NH$_2$ and Ac-HHHHHH-NH$_2$ to form metal complexes. We can observe that, in the case of Cu^{2+} and above pH 4.5, the six consecutive histidines become more effective than seven alternated histidines. The trend is inverted in the case of Zn^{2+} ion, where the peptide Ac-HTHEHSHDHSHAH-NH$_2$ is confirmed to be the best ligand.

4. Materials and methods

4.1. Materials

The investigated peptide Ac-HTHEHSHDHSHAH-NH$_2$ was purchased from KareBay Biochem (USA) with a certified purity of 98% and used as received. Zn(ClO$_4$)$_2$•6H$_2$O and Cu(ClO$_4$)$_2$•6H$_2$O were extra pure products (Sigma-Aldrich). The concentrations of their stock solutions were standardized by EDTA titration and periodically checked via ICP-MS. The carbonate-free stock solution of 0.1 M NaOH was purchased from Sigma-Aldrich and standardized with the primary standard potassium hydrogen phthalate (99.9% purity) by potentiometry. The HClO$_4$ stock solution was prepared by diluting concentrated HClO$_4$ (Sigma-Aldrich) and then standardizing with NaOH. The ionic strength was adjusted to 0.1 M by adding NaClO$_4$ (Sigma-Aldrich). Grade A glassware was employed throughout. All sample solutions were prepared with freshly doubly distilled water.

4.2. Thermodynamic measurements

Stability constants for proton and metal complexes were calculated from pH-metric titration curves registered at T = 298 K and ionic strength I = 0.1 M (NaClO$_4$) using a total volume of 3 mL. The potentiometric apparatus consisted of a Metrohm 905 Titrando pH-meter system provided with a Metrohm LL Unitrode glass electrode and a dosing system 800 Dosino, equipped with a 2 ml micro burette. High purity grade argon was gently blown over the sample solution to ensure
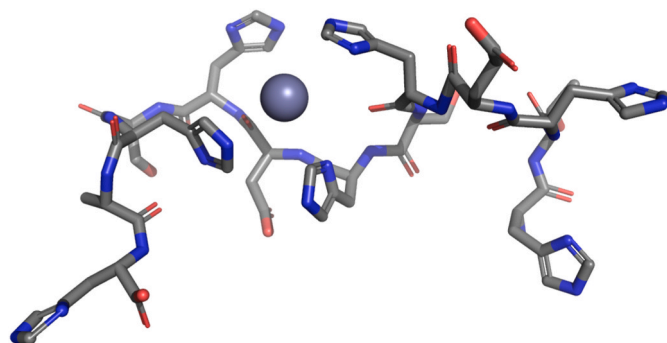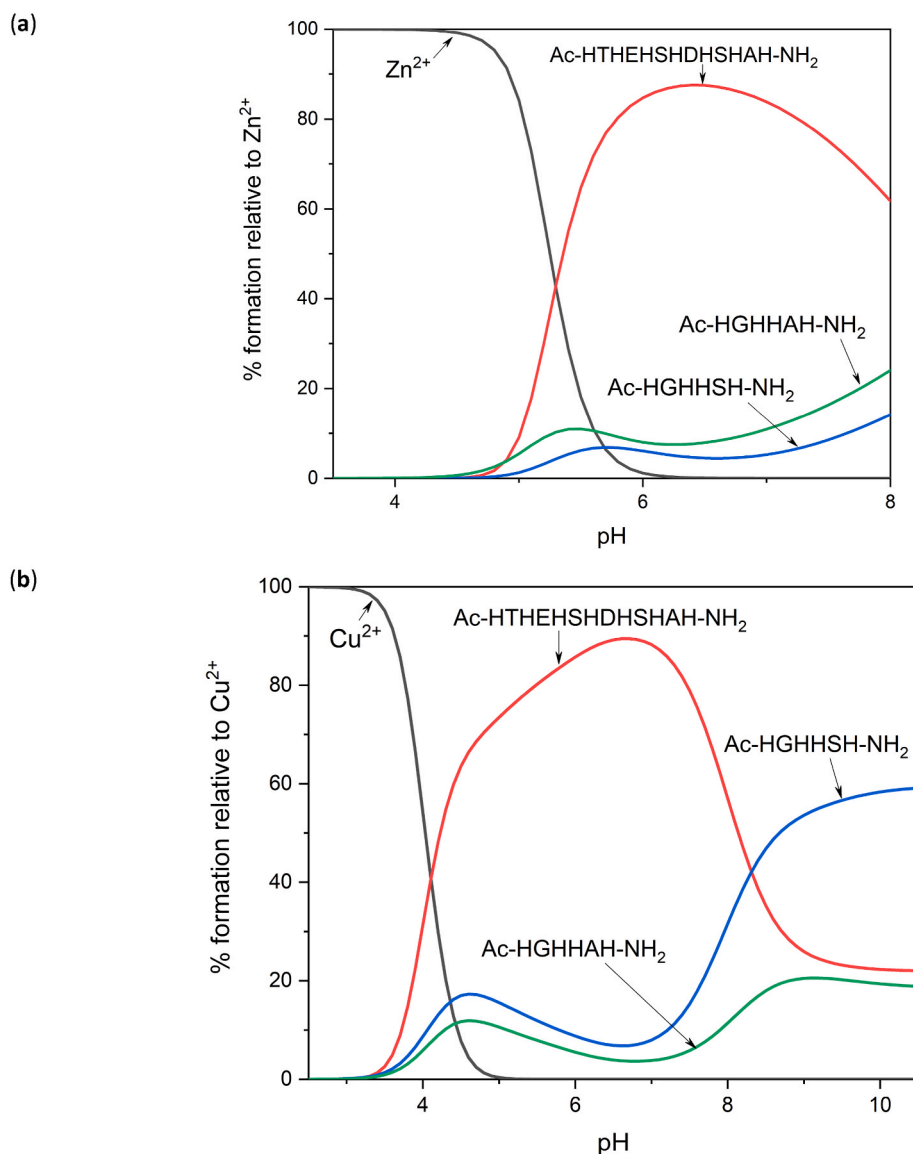
(a)

(b)

Fig. 6. Competition plots for a solution containing equimolar concentrations ($1 \bullet 10^{-3}$ M) of Ac-HTHEHSHDHSHAH-NH$_2$, Ac-HGHHSH-NH$_2$, Ac-HGHHAH-NH$_2$ [31] and (a) Zn^{2+}; (b) Cu^{2+}. The plot is based on the determined thermodynamic constants and describes the formation of the binary metal complexes with each component at different pH values in a simulated solution that contains all reagents in equimolar amount.

an inert atmosphere. Solutions were titrated under constant-speed magnetic stirring with 0.1 M carbonate-free NaOH. The electrode was daily calibrated for hydrogen ion concentration by titrating HClO$_4$ with standard NaOH under the same experimental conditions as above. The standard potential and the slope of the electrode couple were computed by means of the Glee [53] program. Sample solutions were prepared with ligand concentration C$_L$ = $0.5 \bullet 10^{-3}$ M and the metal:ligand ratio was M:L = 0.9:1. The purities and the exact concentrations of the ligand solutions were potentiometrically determined using the Gran method [54]. The HYPERQUAD [55] program was employed to calculate the overall formation constant (β), referring to the following equilibrium:

$$pM + qL + rH \leftrightarrows M_pL_qH_r$$
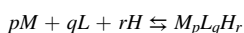
(charges omitted, p is 0 in the case of ligand protonation, r can be negative). Step formation constants (K) and/or acid dissociation constants (K_a) are also reported. The computed standard deviations (referring to random errors only) were given by the program itself and are shown in parentheses as uncertainties on the last significant figure. Hydrolysis constants for Cu^{2+} and Zn^{2+} ions were taken from the

literature [56,57]. The distribution diagrams were computed using the HYSS program [58]. A comparison among the overall metal binding ability of different ligands was performed in different ways. First of all, some competition diagrams were drawn. They represent simulations of solutions containing the metal and the two (or more) ligands and are based on the binary speciation models, admitting that all the components compete to form the respective binary complexes without mixed species formation. In addition, three parameters which give an overall estimation of the metal binding affinity for each peptide at pH 7.4 were computed. K_d (dissociation constant) refers to the generic equilibrium: ML = M + L (charges omitted, M is metal, L is ligand) and corresponds to the concentration of the free metal ion when the half ligand is in a complexed form and half is free. A smaller value of K_d means a greater stability of the formed complexes [59]. The pM value is instead the negative logarithm of the free metal concentration under given experimental conditions (most often: C$_{M,tot}$ = $1 \bullet 10^{-6}$ M, C$_{L,tot}$ = $1 \bullet 10^{-5}$ M) [60]. A high pM value corresponds to a low concentration of free metal ion and thus to a strong ligand. Finally, considering the system from a different point of view, the parameter pL$_{0.5}$ is defined as the amount of ligand required to bind 50% of the metal (typically, a metal quantity as
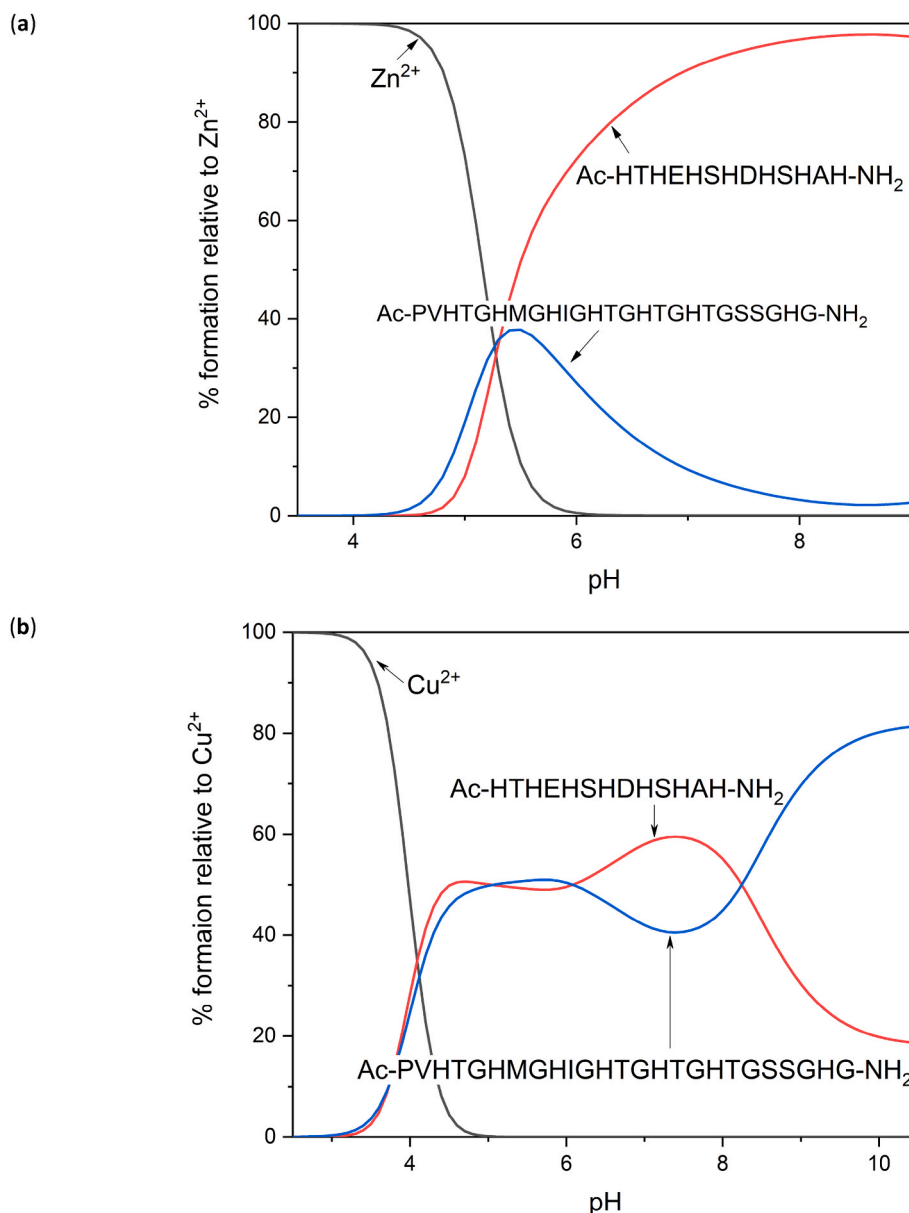
Fig. 7. Competition plots for a solution containing equimolar concentrations ($1\bullet10^{-3}$ M) of Ac-HTHEHSHDHSHAH-NH$_2$, Ac-PVHTGHMGHIGHTGHTGHTGSSGHG-NH$_2$ [51,52] and (a) Zn^{2+}; (b) Cu^{2+}. The plot is based on the determined thermodynamic constants and describes the formation of the binary metal complexes with each component at different pH values in a simulated solution that contains all reagents in equimolar amount.

low as $C_{M,tot} = 1\bullet10^{-12}$ M is considered for this calculation) [61]. Even in this case, the higher the value of pL$_{0.5}$ and the higher is the affinity of the ligand for the metal ion.

4.3. Mass spectrometric measurements

High-resolution mass spectra were obtained on a BrukerQ-FTMS spectrometer (Bruker Daltonik, Bremen, Germany), equipped with an Apollo II electrospray ionization source with an ion funnel. The mass spectrometer operated in the positive ion mode. The instrumental parameters were as follows: scan range *m/z* 100–2500, dry gas nitrogen, temperature 453 K and ion energy 5 eV. The capillary voltage was optimized to the highest signal-to-noise ratio, corresponding to 4500 V. The small changes in voltage (±500 V) did not significantly affect the optimized spectra. The samples (Zn^{2+}:L and Cu^{2+}:ligand in a 0.9:1 stoichiometry, [ligand]$_{tot}$ = 0.5 · 10^{-3} M) were prepared in a 1:1 methanol–water mixture at different pH values and were infused at a flow rate of 3 μL min^{-1}. The instrument was externally calibrated with a

Tunemix™ mixture (Bruker Daltonik, Germany) in quadratic regression mode. Data were processed using the Bruker Compass DataAnalysis 4.2 program. The mass accuracy for the calibration was better than 5 ppm, enabling together with the true isotopic pattern (using SigmaFit) an unambiguous confirmation of the elemental composition of the obtained complex.

4.4. Spectroscopic measurements

The absorption spectra were recorded on a Varian Cary300 Bio spectrophotometer, in the range 200–800 nm, using a quartz cuvette with an optical path of 1 cm. Circular dichroism (CD) experiments were recorded on a Jasco J-1500 CD spectrometer at 298 K in a 0.01 cm and 1 cm quartz cells for the spectral ranges of 180–260 and 200–800 nm, respectively. The ligand was dissolved in a water solution containing $4\cdot10^{-3}$ M HClO$_4$ at 0.1 M ionic strength (NaClO$_4$). Ligand concentration was $0.5\cdot10^{-3}$ M (200–800 nm range) and $0.1\cdot10^{-3}$ M (180–270 nm range). Cu^{2+} to ligand molar ratio was 0.9:1. The UV–Vis and CD
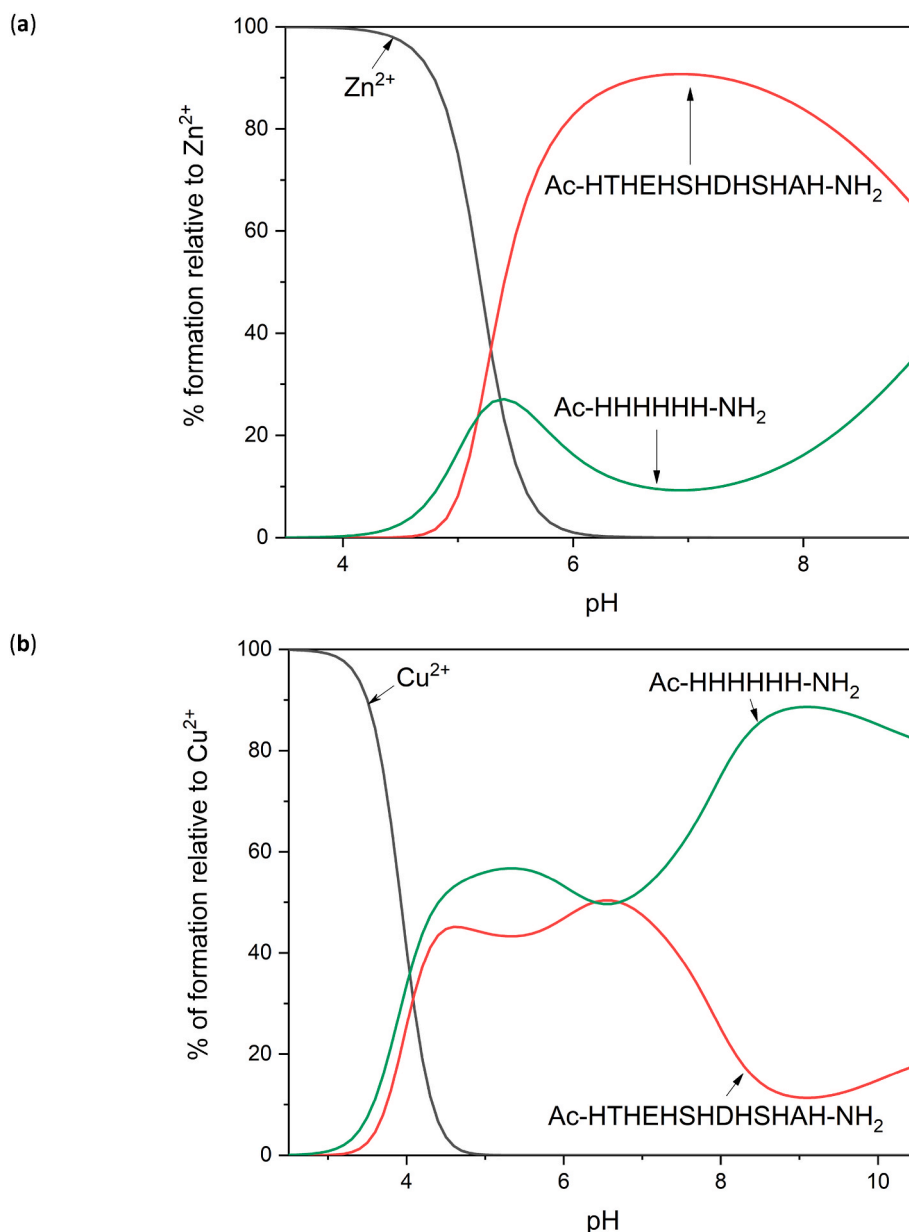
Fig. 8. Competition plots for a solution containing equimolar concentrations ($1 \cdot 10^{-3}$ M) of Ac-HTHEHSHDHSHAH-NH$_2$, Ac-HHHHHH-NH$_2$ [28,33] and (a) Zn^{2+}; (b) Cu^{2+}. The plot is based on the determined thermodynamic constants and describes the formation of the binary metal complexes with each component at different pH values in a simulated solution that contains all reagents in equimolar amount.

spectroscopic parameters were extracted from the spectra obtained at the pH values corresponding to the maximum concentration of each particular species, based on distribution diagrams. Electron paramagnetic resonance (EPR) spectra were recorded in liquid nitrogen on a Bruker ELEXSYS E500 CW-EPR spectrometer at X-band frequency (frequency = 9.578–9.582 GHz, modulation amplitude = 10.00 G) and equipped with an ER 036TM NMR teslameter and an E41 FC frequency counter. Ethylene glycol (30%) was used as a cryoprotectant. Ligand concentration was $1.0 \cdot 10^{-3}$ M and Cu^{2+} to ligand ratio = 0.9:1. The EPR parameters were analysed by simulating the experimental spectra using WIN-EPR SIMFONIA software, version 1.2 (Bruker).

5. Conclusions

Highlighting the metal chelation ability of a protein sequence provides novel insights into the mechanisms of metal homeostasis and in which extent a protein metal-binding site is effective with respect to

many other competitive systems. In fact, it is well-known that bacteria and host organisms compete for the acquisition of metal ions, being involved in a process called nutritional immunity. Therefore, the relative metal binding affinity has an impact on the biological function of the involved systems. The focus of this work is YrpE, a putative zinc binding protein of the Gran-positive bacterium *B. subtilis*, which shows high similarity with ZinT protein.

The mechanism of metal binding to ZinT protein family has been widely investigated in recent years by means of different experimental methods. Both the whole proteins and peptide models have been employed to clarify the way of action and biological role of the systems [31,62,63]. In ZinT protein family, multiple metal binding sites are present, therefore employing peptide models simplified the investigation and provided thermodynamic information on the specific protein domains [31]. This allows to compare the behaviour of metal binding domains of the same or different proteins and experimentally corroborate hypotheses on the mechanism of action. Since the main difference

between YrpE and previously investigated ZinT proteins of *E. coli* and *S. enterica* concerns the N-terminal His-rich loop, we extended the study to this region of YrpE relying on peptide models. The purpose of this experimental method is to provide information that, using the whole protein, would not be possible to obtain. In particular, the aim is to investigate the behaviour of specific metal-binding sites, providing information on the thermodynamic and coordination properties at different experimental conditions (*e.g.* pH). Such information can be obtained only partially or cannot be obtained studying the full-length protein, especially in the presence of multiple metal-binding domains that have different functions and behaviours in a biological context (it is the case of ZinT protein family).

Here, we studied the formation of Zn^{2+} and Cu^{2+} complexes with the peptide Ac-HTHEHSHDHSHAH-NH$_2$, which serves as model for the N-terminal His-rich domain (residues 57–69). The obtained data confirm that this sequence is a very effective ligand for the investigated metal ions. Moreover, the thermodynamic constants are in agreement with theoretical expectations: Cu^{2+} complexes proved to be more stable than Zn^{2+} complexes ($K_d(Cu^{2+}) = 1.37 \cdot 10^{-11}$, $K_d(Zn^{2+}) = 1.24 \cdot 10^{-8}$; Table 2), following the trend based on the Irving–Williams series.

The formed metal complexes are mononuclear polymorphic species, where different sets of donor atoms are possible. In the case of zinc, however, the main species is a ($4N_{Im}$) complex with four histidine bound to the metal. Copper coordination sphere instead changes according to the pH: under acidic conditions there is a prevalence of octahedral complexes with two to five coordinated histidines, while above neutral pH the amide groups of the peptide backbone substitute up to three coordinated histidines in equatorial positions, increasing the square-planar character of the geometry.

Pointing out the similarities and differences between YrpE and *Ec*ZinT/*Se*ZinT N-terminal His-rich domains, we compared the corresponding peptide sequences. Interestingly, our results show that the N-terminal His-rich domain of YrpE binds zinc and copper with higher affinity than the corresponding domain in ZinT proteins. We can explain this behaviour by means of analytical solution equilibria studies of His-containing peptides, confirming that the higher the number of histidines, the higher the stability of the formed complexes. From a biological perspective, it is significant that the most effective metal-binding domain is that of YrpE, supposedly secreted by the Gram-positive bacterium *B. subtilis* and therefore exposed to the extracellular environment. On the other hand, ZinT from *E. coli* and *S. enterica* is located in the periplasm and displays a less efficient His-rich domain.

This work is also aimed at shedding light on the metal-binding abilities of different polyhistidine sequences. The investigation highlights that peptides containing alternated His residues are very effective zinc chelators. In particular, the -(XH)$_n$- motif, where one residue separates each histidine, exhibits a higher zinc binding affinity than the -(XXH)$_n$- motif. The same occurs comparing alternated and consecutive polyhistidine sequences: ligand Ac-HTHEHSHDHSHAH-NH$_2$ is able to bind Zn^{2+} with higher affinity than the His6 tag (HHHHHH). This latter sequence is widely employed in many technological applications, including separation and purification of proteins by chromatography. Nonetheless, natural derived polyhistidine tags are often already used for their better performance.

In conclusion, we obtained the thermodynamic characterization of a new His-rich peptide which shows high zinc binding affinity and serves as model for the study of the metal acquisition by YrpE zinc-binding protein. The opportunities connected to polyhistidine peptides as metal chelators are several, ranging from the design of antimicrobial agents able to withhold metal micronutrients in infected cells, to the development of devices with environmental applications for metal sensing and decontamination. Lastly, the obtained results highlight the efficacy of the employed analytical method to thermodynamically and spectroscopically characterize a protein metal-binding site by means of appropriate model peptides, also allowing the comparison with other complex systems and pointing out properties and behaviours

Table 2
Calculated dissociation constants (K_d), pM and pL$_{0.5}$ values for Zn^{2+} and Cu^{2+} complexes with the ligand Ac-HTHEHSHDHSHAH-NH$_2$, at pH 7.4.

	Zn^{2+}	Cu^{2+}
K_d	$1.24 \cdot 10^{-8}$	$1.37 \cdot 10^{-11}$
pM	8.85	11.64
pL$_{0.5}$	7.89	10.68

inaccessible by other procedures.

Author contributions - CRediT

D.B., M.R.: Conceptualization, Methodology. D.B., A.H., M.R.: Data curation, Writing- Original draft preparation. D.B., S.L.: Visualization, Investigation. D.B., M.R.: Supervision. D.B., S.L., A.H., M.R.: Writing-Reviewing and Editing.

Declaration of competing interest

The authors declare no competing interests.

Data availability

Data will be made available on request.

Acknowledgments

Appendix A. Supplementary data

Supplementary data to this article can be found online at https://doi.org/10.1016/j.ab.2023.115315.

References

[1] P. Faller, C. Hureau, P. Dorlet, P. Hellwig, Y. Coppel, F. Collin, et al., Methods and techniques to study the bioinorganic chemistry of metal–peptide complexes linked to neurodegenerative diseases, Coord. Chem. Rev. 256 (19) (2012) 2381–2396.

[2] A. Hecel, A. Kola, D. Valensin, H. Kozlowski, M. Rowinska-Zyrek, Metal complexes of two specific regions of ZnuA, a periplasmic zinc(II) transporter from Escherichia coli, InCh 59 (3) (2020) 1947–1958.

[3] D. Bellotti, A. Miller, M. Rowińska-Żyrek, M. Remelli, Zn2+ and Cu2+ binding to the extramembrane loop of Zrt2, a zinc transporter of Candida albicans, Biomolecules 12 (1) (2022) 121.

[4] H.A. Hong, R. Khaneja, N.M.K. Tam, A. Cazzato, S. Tan, M. Urdaci, et al., Bacillus subtilis isolated from the human gastrointestinal tract, Res. Microbiol. 160 (2) (2009) 134–143.

[5] Á.T. Kovács, Bacillus subtilis, Trends Microbiol. 27 (8) (2019) 724–725.

[6] J. Olmos, M. Acosta, G. Mendoza, V. Pitones, Bacillus subtilis, an ideal probiotic bacterium to shrimp and fish aquaculture that increase feed digestibility, prevent microbial diseases, and avoid water pollution, Arch. Microbiol. 202 (3) (2020) 427–435.

[7] V. Hlordzi, F.K.A. Kuebutornye, G. Afriyie, E.D. Abarike, Y. Lu, S. Chi, et al., The use of Bacillus species in maintenance of water quality in aquaculture: a review, Aquaculture Reports 18 (2020), 100503.

[8] Y. Gu, X. Xu, Y. Wu, T. Niu, Y. Liu, J. Li, et al., Advances and prospects of Bacillus subtilis cellular factories: from rational design to industrial applications, Metab. Eng. 50 (2018) 109–121.

[9] X. Zhang, A. Al-Dossary, M. Hussain, P. Setlow, J. Li, Applications of Bacillus subtilis spores in biotechnology and advanced materials, Appl. Environ. Microbiol. 86 (17) (2020), e01096-20.

[10] J.-H. Cha, S. Rahimnejad, S.-Y. Yang, K.-W. Kim, K.-J. Lee, Evaluations of Bacillus spp. as dietary additives on growth performance, innate immunity and disease

resistance of olive flounder (Paralichthys olivaceus) against Streptococcus iniae and as water additives, Aquaculture 402–403 (2013) 50–57.

[11] R.O. Yusuf, Z.Z. Noor, M.A.A. Hassan, S.E. Agarry, B.O. Solomon, A comparison of the efficacy of two strains of Bacillus subtilis and Pseudomonas fragii in the treatment of tannery wastewater, Desalination Water Treat. 51 (16–18) (2013) 3189–3195.

[12] F.L.S. de Alencar, J.A. Navoni, V.S. do Amaral, The use of bacterial bioremediation of metals in aquatic environments in the twenty-first century: a systematic review, Environ. Sci. Pollut. Res. 24 (20) (2017) 16545–16559.

[13] M. Wróbel, W. Śliwakowski, P. Kowalczyk, K. Kramkowski, J. Dobrzyński, Bioremediation of heavy metals by the Genus Bacillus, Int. J. Environ. Res. Publ. Health 20 (6) (2023) 4964.

[14] J. Ding, W. Chen, Z. Zhang, F. Qin, J. Jiang, A. He, et al., Enhanced removal of cadmium from wastewater with coupled biochar and Bacillus subtilis, Water Sci. Technol. 83 (9) (2021) 2075–2086.

[15] R.J. Doyle, T.H. Matthews, U.N. Streips, Chemical basis for selectivity of metal ions by the Bacillus subtilis cell wall, J. Bacteriol. 143 (1) (1980) 471–480.

[16] B.S. Alotaibi, M. Khan, S. Shamim, Unraveling the underlying heavy metal detoxification mechanisms of Bacillus species, Microorganisms 9 (8) (2021).

[17] S. Grumbein, M. Opitz, O. Lieleg, Selected metal ions protect Bacillus subtilis biofilms from erosion, Metallomics 6 (8) (2014) 1441–1450.

[18] T.L. Dinh, G.R. Akhmetova, D.S. Martykanova, N.L. Rudakova, M.R. Sharipova, Influence of divalent metal ions on biofilm formation by Bacillus subtilis, BioNanoScience 9 (2) (2019) 521–527.

[19] C.M. Moore, J.D. Helmann, Metal ion homeostasis in Bacillus subtilis, Curr. Opin. Microbiol. 8 (2) (2005) 188–195.

[20] J.R. Morey, T.E. Kehl-Fie, Bioinformatic mapping of opine-like zincophore biosynthesis in bacteria, mSystems 5 (4) (2020), e00554-20.

[21] J. Wątly, S. Potocki, M. Rowińska-Żyrek, Zinc homeostasis at the bacteria/host interface—from coordination chemistry to nutritional immunity, Chem. Eur J. 22 (45) (2016) 15992–16010.

[22] A. Ilari, F. Alaleona, G. Tria, P. Petrarca, A. Battistoni, C. Zamparelli, et al., The Salmonella enterica ZinT structure, zinc affinity and interaction with the high-affinity uptake protein ZnuA provide insight into the management of periplasmic zinc, Biochim. Biophys. Acta 1840 (1) (2014) 535–544.

[23] D.P. Neupane, D. Avalos, S. Fullam, H. Roychowdhury, E.T. Yukl, Mechanisms of zinc binding to the solute-binding protein AztC and transfer from the metallochaperone AztD, J. Biol. Chem. 292 (42) (2017) 17496–17505.

[24] B. Bersch, C. Bougault, L. Roux, A. Favier, T. Vernet, C. Durmort, New insights into histidine triad proteins: solution structure of a Streptococcus pneumoniae PhtD domain and zinc transfer to AdcAII, PLoS One 8 (11) (2013), e81168-e.

[25] D. Bellotti, M. Rowińska-Żyrek, M. Remelli, How zinc-binding systems, expressed by human pathogens, acquire zinc from the colonized host environment: a critical review on zincophores, Curr. Med. Chem. 28 (35) (2021) 7312–7338.

[26] E.M. Panina, A.A. Mironov, M.S. Gelfand, Comparative genomics of bacterial zinc regulons: enhanced ion transport, pathogenesis, and rearrangement of ribosomal proteins, Proc. Natl. Acad. Sci. USA 100 (17) (2003) 9912–9917.

[27] E. Székely, G. Csire, B.D. Balogh, J.Z. Erdei, J.M. Király, J. Kocsi, et al., The role of side chains in the fine-tuning of the metal-binding ability of multihistidine peptides, Molecules [Internet] 27 (11) (2022).

[28] J. Wątly, A. Hecel, M. Rowińska-Żyrek, H. Kozłowski, Impact of histidine spacing on modified polyhistidine tag – metal ion interactions, Inorg. Chim. Acta. 472 (2018) 119–126.

[29] M. Varadi, S. Anyango, M. Deshpande, S. Nair, C. Natassia, G. Yordanova, et al., AlphaFold Protein Structure Database: massively expanding the structural coverage of protein-sequence space with high-accuracy models, Nucleic Acids Res. 50 (D1) (2022) D439–D444.

[30] The UniProt Consortium, UniProt: the universal protein knowledgebase, Nucleic Acids Res. 46 (5) (2018) 2699.

[31] D. Bellotti, M. Rowińska-Żyrek, M. Remelli, Novel insights into the metal binding ability of ZinT periplasmic protein from Escherichia coli and Salmonella enterica, Dalton Trans. 49 (27) (2020) 9393–9403.

[32] T.R. Cawthorn, B.E. Poulsen, D.E. Davidson, D. Andrews, B.C. Hill, Probing the kinetics and thermodynamics of copper(II) binding to Bacillus subtilis sco, a protein involved in the assembly of the CuA center of cytochrome c oxidase, Biochemistry 48 (21) (2009) 4448–4454.

[33] J. Watly, E. Simonovsky, R. Wieczorek, N. Barbosa, Y. Miller, H. Kozlowski, Insight into the coordination and the binding sites of Cu2+ on the histidyl-6-tag using experimental and computational tools, Inorg. Chem. 53 (13) (2014) 6675–6683.

[34] S.E. Conklin, E.C. Bridgman, Q. Su, P. Riggs-Gelasco, K.L. Haas, K.J. Franz, Specific histidine residues confer histatin peptides with copper-dependent activity against Candida albicans, Biochemistry 56 (32) (2017) 4244–4255.

[35] D. Bellotti, M. Toniolo, D. Dudek, A. Mikołajczyk, R. Guerrini, A. Matera-Witkiewicz, et al., Bioinorganic chemistry of calcitermin – the picklock of its antimicrobial activity, Dalton Trans. 48 (36) (2019) 13740–13752.

[36] M. Mihailescu, M. Sorci, J. Seckute, V.I. Silin, J. Hammer, B.S. Perrin Jr., et al., Structure and function in antimicrobial piscidins: histidine position, directionality of membrane insertion, and pH-dependent permeabilization, J. Am. Chem. Soc. 141 (25) (2019) 9837–9853.

[37] C. Remuzgo, T.S. Oewel, S. Daffre, T.R.S. Lopes, F.H. Dyszy, S. Schreier, et al., Chemical synthesis, structure–activity relationship, and properties of shepherin I: a fungicidal peptide enriched in glycine-glycine-histidine motifs, Amino Acids 46 (11) (2014) 2573–2586.

[38] I.H. Lee, C. Zhao, Y. Cho, S.S.L. Harwig, E.L. Cooper, R.I. Lehrer, Clavanins, α-helical antimicrobial peptides from tunicate hemocytes, FEBS Lett. 400 (2) (1997) 158–162.

[39] M.I. Hood, E.P. Skaar, Nutritional immunity: transition metals at the pathogen–host interface, Nat. Rev. Microbiol. 10 (2012) 525–537.

[40] S. Damo, T.E. Kehl-Fie, Metal sequestration: an important contribution of antimicrobial peptides to nutritional immunity, in: J. Harder, J.-M. Schröder (Eds.), Antimicrobial Peptides: Role in Human Health and Disease, Springer International Publishing, Cham, 2016, pp. 89–100.

[41] R.C.F. Cheung, J.H. Wong, T.B. Ng, Immobilized metal ion affinity chromatography: a review on its applications, Appl. Microbiol. Biotechnol. 96 (6) (2012) 1411–1420.

[42] R. Irankunda, J.A. Camaño Echavarría, C. Paris, L. Stefan, S. Desobry, K. Selmeczi, et al., Metal-chelating peptides separation using immobilized metal ion affinity chromatography: experimental methodology and simulation, Separations 9 (11) (2022) 370.

[43] B. Godat, L. Engel, N.A. Betz, T.M. Johnson, Methods for the purification of HQ-tagged proteins, in: M. Zachariou (Ed.), Affinity Chromatography: Methods and Protocols, Humana Press, Totowa, NJ, 2008, pp. 151–168.

[44] G. Chaga, D.E. Bochkariov, G.G. Jokhadze, J. Hopp, P. Nelson, Natural poly-histidine affinity tag for purification of recombinant proteins on cobalt(II)-carboxymethylaspartate crosslinked agarose, J. Chromatogr. 864 (2) (1999) 247–256.

[45] L.D. Pettit, H.K.J. Powell, The IUPAC Stability Constants Database, Royal Society of Chemistry, London, 1992-2000.

[46] H. Sigel, R.B. Martin, Coordinating properties of the amide bond. Stability and structure of metal ion complexes of peptides and related ligands, Chem. Rev. 82 (4) (1982) 385–426.

[47] K. Ősz, B. Bóka, K. Várnagy, I. Sóvágó, T. Kurtán, S. Antus, The application of circular dichroism spectroscopy for the determination of metal ion speciation and coordination modes of peptide complexes, Polyhedron 21 (21) (2002) 2149–2159.

[48] H.F. Stanyon, X. Cong, Y. Chen, N. Shahidullah, G. Rossetti, J. Dreyer, et al., Developing predictive rules for coordination geometry from visible circular dichroism of copper(II) and nickel(II) ions in histidine and amide main-chain complexes, FEBS J. 281 (17) (2014) 3945–3954.

[49] M. Sola, A. Lledos, M. Duran, J. Bertran, Anion binding and pentacoordination in zinc(II) complexes, Inorg. Chem. 30 (11) (1991) 2523–2527.

[50] L. Casella, M.E. Silver, J.A. Ibers, Synthesis and characterization of copper(I), copper(II), zinc(II), cobalt(II), and iron(II) complexes of a chelating ligand derived from 2,6-diacetylpyridine and L-histidine. Oxygenation of the copper(I), cobalt(II), and iron(II) complexes. Crystal structure of the zinc(II) complex, Inorg. Chem. 23 (10) (1984) 1409–1418.

[51] L. Szyrwiel, E. Jankowska, A. Janicka-Klos, Z. Szewczuk, D. Valensin, H. Kozlowski, Zn(II) ions bind very efficiently to tandem repeat region of "prion related protein" (PrP-rel-2) of zebra-fish. MS and potentiometric evidence, Dalton Trans. 44 (2008) 6117–6120.

[52] D. Valensin, L. Szyrwiel, F. Camponeschi, M. Rowinska-Zyrek, E. Molteni, E. Jankowska, et al., Heteronuclear and homonuclear Cu2+ and Zn2+ complexes with multihistidine peptides based on zebrafish prion-like protein (vol 48, pg 7340, 2009), Inorg. Chem. 48 (18) (2009) 9042.

[53] P. Gans, B. O'Sullivan, GLEE, a new computer program for glass electrode calibration, Talanta 51 (1) (2000) 33–37.

[54] G. Gran, Determination of the equivalent point in potentiometric titrations, Acta Chem. Scand. 4 (1950) 559–577.

[55] P. Gans, A. Sabatini, A. Vacca, Investigation of equilibria in solution. Determination of equilibrium constants with the HYPERQUAD suite of programs, Talanta 43 (10) (1996) 1739–1753.

[56] G. Arena, R. Cali, E. Rizzarelli, S. Sammartano, Thermodynamic study on the formation of the cupric ion hydrolytic species, Thermochim. Acta 16 (3) (1976) 315–321.

[57] P.L. Brown, C. Ekberg, First transition series metals, Hydrolysis of Metal Ions (2016) 499–716.

[58] L. Alderighi, P. Gans, A. Ienco, D. Peters, A. Sabatini, A. Vacca, Hyperquad simulation and speciation (HySS): a utility program for the investigation of equilibria involving soluble and partially soluble species, Coord. Chem. Rev. 184 (1999) 311–318.

[59] H. Kozlowski, M. Łuczkowski, M. Remelli, Prion proteins and copper ions. Biological and chemical controversies, Dalton Trans. 39 (28) (2010) 6371–6385.

[60] D. Bellotti, A. Sinigaglia, R. Guerrini, E. Marzola, M. Rowińska-Żyrek, M. Remelli, The N-terminal domain of Helicobacter pylori's Hpn protein: the role of multiple histidine residues, J. Inorg. Biochem. 214 (2021) 111304.

[61] F. Crea, C. De Stefano, C. Foti, S. Milea, S. Sammartano, Chelating agents for the sequestration of mercury(II) and monomethyl mercury(II), Curr. Med. Chem. 21 (33) (2014) 3819–3836.

[62] P. Petrarca, S. Ammendola, P. Pasquali, A. Battistoni, The Zur-regulated ZinT protein is an auxiliary component of the high-affinity ZnuABC zinc transporter that facilitates metal recruitment during severe zinc shortage, J. Bacteriol. 192 (6) (2010) 1553–1564.

[63] J. Chen, L. Wang, F. Shang, Y. Dong, N.-C. Ha, K.H. Nam, et al., Crystal structure of E. coli ZinT with one zinc-binding mode and complexed with citrate, Biochem. Biophys. Res. Commun. 500 (2) (2018) 139–144.